Photo-active and Dynamical Properties of Hematite (Fe_2O_3)-Water Interfaces: An Experimental and Theoretical Study

Niall J. English[1,2,*], Mahfujur Rahman[1*], Nitin Wadnerkar[2,*],and J.M.D. MacElroy[1,2*]

[1] *The SEC Strategic Research Cluster and the, School of Chemical and Bioprocess Engineering, University College Dublin, Belfield, Dublin 4, Ireland*

[2]*The Centre for Synthesis and Chemical Biology ,School of Chemical and Bioprocess Engineering, University College Dublin, Belfield, Dublin 4, Ireland*

Keywords: Molecular Dynamics, Iron Oxide, Water, Density Functional Theory, Adsorption

The dynamical properties of physically and chemically adsorbed water molecules at pristine hematite-(001) surfaces have been studied by means of equilibrium Born-Oppenheimer molecular dynamics (BOMD) in the NVT ensemble at 298 K. The dissociation of water molecules to form chemically adsorbed species was scrutinised, in addition to 'hopping' or swapping events of protons between water molecules. Particular foci have been dynamical properties of the adsorbed water molecules and OH^- and H_3O^+ ions, the hydrogen bonds between protons in water molecules and the bridging oxygen atoms at the hematite surface, as well as the interactions between oxygen atoms in adsorbed water molecules and iron atoms at the hematite surface. Experimental results for photoelectrical current generation complement simulation findings of water dissociation.

*Corresponding Author

Tel: + 353-1-716-1646 (NE), -1824 (J.M.D. MacE); Fax: + 353-1-716-1177 (NE& J.M.D. MacE)
E-mail:tipu.ucd@gmail.com (MR), wadnerkar_nitin@yahoo.com (NW), niall.english@ucd.ie (NE), don.macelroy@ucd.ie (J.M.D. MacElroy)

Introduction

Since the discovery of Fujishima and Honda that TiO_2 (titania) could split water under light irradiation to produce hydrogen and oxygen gas [1], the study of the properties of aqueous solutions in contact with metal oxide interfaces has undergone a substantial increase in scrutiny. There are many potential applications for renewable energy using photo-electrochemical water splitting for a range of other semiconductor-water interfaces, and not only for TiO_2, although titania is abundant, inexpensive and non-toxic. Often, these will exploit support-metal-support-interaction (SMSI) modification of photo-catalytic properties [2]. Although TiO_2 is one of the most studied metal oxides in the literature, α-Fe_2O_3 has come to be of equal, if not more, interest in recent years, due to its relative ubiquity and low cost, with a seemingly ideal bad gap [3-10]. However, despite recent progress in our understanding of titania-water interfaces [11,12], including via theoretical and molecular simulation methods [13], the successful modelling of hematite-water interfaces remains rather challenging and elusive.

Such metal oxide-water interfaces provide a rich environment for study of the dynamical properties of confined water molecules; this is particularly so where hydrogen-bonded molecules play an important role in stabilising solutes via solvent interactions and in forming "cages". Molecular dynamics (MD) has been useful to some extent in characterising the dynamical and vibrational behaviour of adsorbed water molecules on metal oxide surfaces, e.g., titania-water [14-23], given titania's status as the putative, or ideal, aspirant 'prototype' material for solar water-splitting. In the case of titania-water, these studies have included orientations of surface-water dipoles [15], their vibrational spectra [16], kinetics of their hydrogen bonding arrangements [17], ion adsorption [18], electric double layer structure [19-21], surface protonation effects [22], and spatial distribution functions [23]. In terms of Density Functional Theory (DFT)-level calculations

for titania-water interfaces, particularly from *ab initio* MD (AIMD), a range of surfaces have been simulated from partial to full coverage, and multiple water layers [13,24]. The influence of defects on anatase-101 surfaces on water adsorption energies has been studied at defective sites [25]. Hydroxide ions have also been studied at these surfaces [26]. Car-Parrinello MD (CPMD) simulations of pristine and defective anatase-101 surfaces have been performed with one, two and three layers of water adsorbed thereon [27], with other CPMD work leading to different surface reconstruction of rutile-011 than under vacuum or low-coverage conditions [28]. AIMD has also offered key insights into the librational motion of higher-frequency modes of water adsorbed to titania in recent studies [29, 30].

The application of MD, whether using classical pairwise potentials or DFT, to interfaces between iron oxide and water has been far less studied, despite the potentially promising prospect of iron oxide for photo-driven water-splitting. More specifically, the 001-surface has been found experimentally to be stable and usually exposed in natural hematite crystals [31, 32]. Rohrbach *et al.* [31] and Bergermayer *et al.* [32] have used DFT to characterise the structure and composition of these (dry) surfaces. Yin *et al.* [33] and Trainor *et al.* [34] have applied DFT to study the adsorption of water on hematite surfaces, and these are in agreement in experiment which show that hydroxylated terminations are more stable. Kubicki *et al.* [35] have examined 010 surfaces of goethite (α-FeOOH) using the PBE functional, paying particular attention to surface complexation models as a function of solvation. Nguyen *et al.* [36] have improved the DFT treatment of hematite-water interfaces by use of PBE+U. In many cases, very low energy barriers were found for water dissociation on hematite-001 surfaces, confirming experimental reports of widespread room-temperature dissociation of water on hematite-001 [36]; this is in some contrast to the debate as to the dominance of physical or chemical water adsorption on rutile-110 at room

temperature [37-39]. However, to the best of our knowledge, there has been no AIMD study of the water-hematite interface, which is needed to capture the rich physic-complexity of room-temperature chemical adsorption and the dynamical properties of the surface hematite layers, along with those of the water. Certainly, the relatively low energy barriers for water dissociation indicated by Nguyen *et al.* [36] suggest that water dissociation may be observable over picosecond timescales in room-temperature AIMD.

Bearing this in mind, the overarching focus of this study is to carry out AIMD simulations of α-Fe_2O_3 (hematite)-001surfaces in contact with (initially) physically adsorbed, full bulk layers of water (as opposed to a somewhat artificial simple water monolayer or bilayer) to assess, *inter alia*, the nature of water dissociation thereon. The evolution of chemical and physical adsorption behaviour, together with consideration of vibrational properties of water-bridging oxygen hydrogen bonds, are also important observables. In parallel, we have also carried out experiments to characterise photo-driven electrical current flows on α-hematite, to underline simulation results for water dissociation at the surface. It must be noted, however, that the AIMD simulations describe *ground-state* dissociation, rather than photo-driven water-splitting, so some care is required in direct correlation of both (experimentally- and theoretically-studied) phenomena.

Experimental Methods

Hematite (α-Fe_2O_3) thin films were prepared on fluorine-doped tin oxide (FTO) glass substrates (TEC 15 from Solaronix, Switzerland) by a custom-made atmospheric-pressure chemical vapour deposition (APCVD) system, and further details may be obtained in ref. 40. Briefly, the APVCD deposition chamber consists of: (i) vapour precursors and an air-delivery system, (ii) a closed-glass deposition chamber, (iii) a substrate heater, and (iv) an exhaust line. Before thin-film

deposition, the conductive glass substrates were cleaned ultrasonically in acetone followed by methanol, each for 5 minutes and drying via blowing dry air. The substrate was placed on the hot-plate and heated to 480 ^{0}C. The temperature of the substrate surface was monitored by a thermocouple. Vapour of iron pentacarbonyl (Fe $(CO)_5$, Aldrich, 99.999%) was used as a source for iron, by bubbling argon gas (99.9999%) through a bubbler containing liquid precursors at a flow rate of 12.5 µl/min. Dry air, as an oxygen source, was then mixed at a flow rate of 2 l/min with the $Fe(CO)_5$ vapour and directed towards the substrate though a glass nozzle with a diameter of 6.0 mm. The dry air serves to minimise the extent of surface-hydroxylation of the hematite, rendering it as anhydrous as possible; the central underlying motivation was to form stoichiometric, 'fine-structured' hematite in the absence of water – *a fortiori*, this corresponds to choosing an initially anhydrous surface in our dynamics simulations, though – *vide infra*. Clearly, however, some level of surface-hydroxylation will be present, especially in view of the relative ease with which (even ground-state) water dissociation can occur (see the discussions on the simulation results). However, the formation of OH^- at the hematite surface would be promoted in the presence of an alkaline electrolyte solution, as used in this study, so there are clearly some OH^- groups present (as was observed during AIMD – *vide infra*). For improving the conductivity of hematite films, in addition to the Fe $(CO)_5$ vapour, TEOS vapour was also supplied as a source for Si dopant , by bubbling argon gas (99.9999%) through liquid precursors with a constant flow rate of 25 µl/min. The substrate surface-to-nozzle distance was kept constant at 20 mm. The deposition time for all coatings was kept constant to 8 min. The flow rate of gases in this work was controlled by a mass flow controller. Before deposition of the hematite layer, a nanoscale-thick SiO_2 layer (of approximately 1 nm thickness, as confirmed by ellipsometry) was deposited

onto the glass substrate, to act as a passive layer for improving charge transportation [41], with an argon gas flow rate of 18 µl/min through tetraethyl orthosilicate (TEOS) precursor for 1 min.

The crystallinity of the hematite coatings was examined by a Siemens D500 X-ray diffractometer (XRD) operating at 40kV and 30mA with Cu K_α radiation at a wavelength of 0.1542nm. The scan was conducted in 2Θ mode and spanned across a range of 20–60° with a step resolution of 0.02°. The photocurrent density, being proportional to the rate of the water-splitting reaction to hydrogen and oxygen on the photo-cathode and anode, respectively, was used as a means of gauging water-splitting in the photo-electrochemical (PEC) cell. The measurements of photocurrent were carried out using a custom-made (PEC) cell, a GamryG300 potentiostat and a Newport 450 W (xenon arc lamp) solar simulator [42, 43]. The PEC cell consists of a working electrode (APCVD-deposited hematite coating), a counter electrode (platinum wire) and a reference saturated calomel electrode (SCE) immersed in an aqueous electrolyte solution of 1 M NaOH, with a pH of 13.6. All potentials were reported against the reversible hydrogen electrode (RHE). A gas chromatography system (HP6890 Series Plus with HP Plot column) was used to detect the hydrogen gas evolved during solar water-splitting process.

Simulation Methodology

We have performed circa 11 ps of NVT equilibrium Born-Oppenheimer molecular dynamics (BOMD) under three-dimensional periodic boundary conditions (PBC) for a condensed state of liquid water over a mobile slab of pristine, initially anhydrous hematite-(001) Fe_2O_3surface. The hematite-(001) surface was cleaved as a 2×1×1 orthorhombic simulation cell (x = 10.076, y = 8.726, z = 13.772 Å) from bulk alpha-hematite (space group 167, H3c) to yield a non-polar and dipole-free surface, and the direction of heterogeneity was the z-axis. The hematite contained 120

atoms. 40 liquid-state water molecules were placed at a density of approximately 1 g/cm^3 in contact with the hematite, with the same *x-y* simulation cell cross-section and a water layer thickness of circa 13 Å. The layer in contact with the hematite was adsorbed physically, using a motif from molecular mechanics energy-optimisation at 0 K with the SPC/E water model [44] and a rigid hematite slab with charges of +1.5 e on the iron ions and -1 e on each oxygen ion.

Three-dimensional periodic DFT was used for each step of BOMD, as implemented in the Vienna *Ab initio* Simulation Package (VASP) [45, 46]. The projected augmented wave (PAW) method was chosen to represent electron-ion interactions [46]. The exchange-correlation interactions were handled by the Perdew-Burke-Ernzerhof generalised gradient approximation (GGA) approach [47]. Γ-point sampling was used, given the reasonably large size of the periodic system, and water layer in the *z*-direction. The plane wave cut-off energy was set to 400 eV. Prior to BOMD and after molecular mechanics optimisation, both the atomic positions and lattice parameters were optimised using the GGA method until the atomic forces were smaller than 0.02eV/Å. A Nosé-Hoover NVT ensemble at 298 K using Verlet integration with a 0.5fs timestep was used,with a relatively mild thermostat coupling period of 0.5 ps [48]. 11 ps of NVT BOMD was run at 298 K. In addition, to compare bulk-liquid water dynamical properties, a cubic simulation box composed of 96 molecules was prepared by classical simulation, and we carried out bulk-liquid-water BOMD for ~9 ps.

To probe dynamical properties, autocorrelation functions (ACFs) were defined for velocities or other quantities for each water molecule or oxygen/hydrogen atoms therein (especially for the case of dissociation), or for O/Fe atoms. In general, a normalised ACF of a quantity $q(t)$ is [48]

$$\mathrm{ACF} = \langle q(0)q(t)\rangle / \langle q(0)q(0)\rangle \quad (1)$$

where brackets denote ensemble-averaging. This gives an indication of the probability that a quantity is correlated with itself as a function time; once sufficient time has elapsed, this probability will have decayed from 1 initially to essentially zero [48]. The normalised velocity-ACF (VACF) of an atom (or particular groups of atoms, α), $c^{\alpha}(t)$, is

$$c^{\alpha}(t) = \left\langle \mathbf{v}_i^{\alpha}(t) \cdot \mathbf{v}_i^{\alpha}(0) \right\rangle \Big/ \left\langle \mathbf{v}_i^{\alpha}(0) \cdot \mathbf{v}_i^{\alpha}(0) \right\rangle \qquad (2)$$

The 'power spectrum' of a (V)ACF is the real (cosine) part of the numerical Fourier transform; the underlying frequency modes characteristic of time-variations may be gleaned therefrom [48]. In (crystalline) solids, this is often termed the 'density of states', and it describes phonon modes, which may also be probed by lattice dynamics methods (although not adjusted for finite temperatures, often making over-simplifications in potential energy). It is also possible to investigate coupling between various quantities, *e.g.*, velocities of the upper layer of Fe and O atoms in the hematite with water by computing velocity cross-correlation functions (VCCFs), where one of the sets of atoms in eqn. 2 is replaced with another, *e.g.*, β [48].

It ought to be noted that for VACF-spectra, the level of expected variability of vibrational frequencies with respect to experiment is estimated to be significant (of the order of 50 cm^{-1}, perhaps more). This is reflected in part by statistical limitations and also the appropriateness of the functional (PBE); the lack of a more refined implementation of dispersion interactions is a drawback. The objective of this study is not to gain (semi-)quantitative agreement with experiment, but rather to probe how physical adsorption alters (water) dynamical properties.

Results and Discussion

The XRD spectra of the hematite thin films are given in Fig. 1 illustrating the crystalline nature of the deposited film with a (110)-diffraction plane peak observed from XRD; there is good

agreement with respect to the JCPDS 00-001-1053 reference peaks for pure hematite. For hematite, electron conduction is strongly favoured along the (001) basal plane with hole conduction taking place within the (110) plane. In order to assess water-splitting on the hematite-water interface, photo-current densities were obtained. The measurements were carried out under interrupted solar-simulator light-on/off as a function of applied potential (E_{app}= -1 V to +1 V SCE) in 1M NaOH aqueous solution. The photo-current was observed for the hematite electrode in the presence of light, as shown in Fig. 2. For a photocurrent of ~1.95 mA/cm2 at 1.23 V vs. the RHE (cf. Fig. 2), the solar-to-hydrogen conversion [49] was measured to be 2.4 %. The photo-electrochemical water-splitting process was also observed visually on the electrode-water interface in presence of simulated sunlight (with a small amount of applied voltage) as shown in snapshot in Fig. 3b. However, no water-splitting was observed under the same conditions when the light was off (cf. Fig. 3a), indicating that the water-splitting process starts in the presence of light. A small amount of voltage required to initiate water-splitting in the presence of light, could be obtained from a stand-alone solar device if the photo-electrochemical cell is constructed in a tandem configuration by adding a low-cost photovoltaic cell such as a dye-sensitised solar cell [50]. The production of oxygen and hydrogen from the respective hematite and Pt electrode-water interfaces were confirmed by gas chromatography (GC). The gas was collected by placing funnels on the electrodes and the funnels were then connected to a burette and septum. Gas samples were then collected using an air-tight syringe (250 µL) from the burette through a septum. A detail of the gas collection and measurement is found elsewhere [51].

[insert Figs. 1-3 about here]

As an aid toward a better understanding of the above observations it is appropriate to investigate theoretically the dynamics of water break-up at hematite surfaces, albeit in the ground-state; this allows the investigation and confirmation of the molecular mechanisms underlying previous experimental and simulation investigations of the ready hydroxylation of hematite 001-surfaces [31, 32, 35, 36]. Snapshots of the interfaces at various times are shown in Fig. 4, whilst a film has been deposited in Supplementary Information, animating the water break-up process and interface dynamics, including surface-hydroxylation, at 0.25-ps intervals. It is evident that strong electrostatic contacts, or ionic 'bonds' develop from the very outset of the MD simulation, and these are shown explicitly between the three surface Fe atoms and oxygen atoms in three water molecules. After ~0.5ps, a 'shaded' water molecule has become more H_3O^+ in character, with 'electrostatically bound' water molecules tending to give up protons thereto (thus becoming more OH^--like, transiently). After ~0.6ps, the shaded, transient H_3O^+ species is attracted (electrostatically) to a hematite surface oxygen atom, whereupon it 'donates' one of its protons thereto to form a chemical bond (achieving initial, partial hydroxylation of the hematite surface). After this, this structure remains essentially stable, having achieved 'formal' hydroxylation with the shaded proton in Fig. 4, but also *de facto* surface modification by physico-chemical electrostatic 'bonds' with either water molecules or OH^- moieties, which exchange protons with surrounding water molecules. It is also to be noted that after ~2-3 ps, there is greater dipolar alignment of the water molecules at the 'top' of the simulation box, which form transient hydrogen bonds (which tend to break and re-form) with the oxygen atoms at the 'bottom' of the hematite surface (shown in Fig. 4(1)); the required reorientation of the water molecules from the initial bulk-like water configuration takes ~3 ps. As an example, in snapshot (6), the dipole

vectors of the water molecules at the 'top' of the box are shown in green, with four of the five aligned approximately towards the bottom of the hematite surface.

[insert Fig. 4 about here]

Although a picture of partial hydroxylation, surface modification, and hematite-induced proton exchange in water has emerged *grosso modo* from consideration of the salient features of Fig.4, it is certainly worthwhile to probe this in greater detail, particularly vis-à-vis dynamical properties and structural considerations. The water-oxygen density profile with respect to *z*-axis position is shown in Fig. 5; the grey lines denote the initial configuration (before any geometry-optimisation), whilst the dotted black line is derived from the trajectory after the first picosecond (*i.e.*, in the relatively stable post-hydroxylation structure). In this latter case, the closer contact of 'water' molecules (or OH^- moieties) with Fe due to electrostatic interactions is clear, with greater evidence of more pronounced hematite-induced 'layering' in the water structure relative to the bulk liquid; this is also the case with a distinct layer at ~24-26 Å at the second interface with the 'bottom' hematite surface in Fig. 4(1). Some evidence of partial layering has also been evident in larger-scale, classical MD studies of periodically-imaged water-titania interfaces, although in the immediate vicinity of the titania [15]. In any event, the distance of only ~13 Å for the water in between the 'top' and 'bottom' periodic images of the hematite lead to the establishment of layering, due to strong, stable electrostatic interactions with the hematite in the immediate adsorption layer effectively immobilising these water molecules translationally, and setting up an electric double layer which penetrates into the water layer in the middle of the two interfaces.

[insert Fig. 5 about here]

The vibrational density of states (from maximum-peak-normalised VACF power spectra, cf. eqn. 1) of the Fe and O atoms in hematite in the 'top' layer in contact with the physically- and chemically-adsorbed water molecules are shown in Fig. 6, after 1 ps. It can be seen that the lowest-lying acoustic-translational phonon peak at *circa* 90 cm^{-1} for Fe atoms couples with O atoms at ~95 cm^{-1}, with a further peak for Fe at ~185 cm^{-1}. Considering O, the lowest-lying acoustic-vibrational peak lies at around 250 cm^{-1}, with a further one at ~460 cm^{-1}. Examining the potential coupling of certain possible vibrational modes with those of the physically adsorbed stable water molecules, H_3O^+ or OH^- species is instructive. In the case of stable water molecules, Fig. 7 depicts the density of states, along with that of bulk liquid water, which, for comparison, is in reasonable agreement with the PBE AIMD work of Pascal *et al.* [52]. The dotted line is the closest water molecule (for which there is stable hydrogen-bonding with the bridging oxygen, and electrostatic interaction with nearby Fe atoms) which stays intact; the dotted grey is another water molecule around 2 Å 'further out' which also stays intact, where these more explicit interactions with the hematite are much weaker. A molecule near the 'middle' of the liquid layer in between the two interfaces is also shown. Coupling of the closest (intact) water molecule 'physically' adsorbed (in a *de facto*, stable ionic bond with a surface Fe atom) is readily evident by the overlap of its O atom frequency modes at ~90 and ~185 cm^{-1} with those of Fe, with other vibrational peaks at ~315 and 390 cm^{-1} also overlapping with corresponding Fe vibrational modes in Fig. 6. In contrast, a sample water molecule around 2 Å further distant from the surface (in dashed grey) displays weaker coupling of its O atom with the Fe acoustic-translational peaks at ~90 and ~185 cm^{-1}, and little in terms of similar acoustic-vibrational modes. The development of a 'continuum-

nature' of the liquid-state spectrum is also seen in the spectrum of the water molecule 'midway' between the two periodically-imaged interfaces. Examination of the power spectra of the corresponding velocity cross correlation functions (VCCFs) for the relevant oxygen atoms in water and the Fe confirmed this coupling for the 'electrostatically-bound' (but, nonetheless, physically adsorbed) intact water molecule.

[insert Figs. 6 and 7 about here]

Turning to the H_3O^+ or OH^- species, their power spectra are discussed with reference to Fig. 8, in terms of their constituent O atoms (reflective of their respective translational density of states). An example, more stable, OH^- ion is physically adsorbed via an electrostatic bond with Fe (cf. Fig. 4), whilst the dashed-grey curve depicts a sample H_3O^+ ion hydrogen-bonded to a bridging oxygen atom at the hematite surface, in a stable configuration. Also, the continuous-black curve depicts a sample H_3O^+ ion around 1.5 Å further from the surface than the directly hydrogen-bonded H_3O^+ ion, with less explicit physical interaction (*i.e.*, no hydrogen bond with a bridging oxygen atom in the hematite surface). It was found that there is substantial coupling of the sample stable OH^- ion with the Fe atom's translational-acoustic modes at ~90 and ~185 cm^{-1}, with some overlap of vibrational-acoustic modes at ~315 and 390 cm^{-1} (cf. Fig. 5); this was confirmed further by the respective VCCF analysis. From inspection of Figs. 5 and 8, there is greater overlap of the H_3O^+ ions with the surface O (bridging) atoms in the hematite, and more especially so for the nearer one (shown in dashed-grey) which is hydrogen-bonded thereto. These observations underpin the strong extent of translational and vibrational coupling with the hematite surface, especially mediated by strong electrostatic and hydrogen-bonding interactions. The reduction in translational

freedom of the adsorbed species is underlined by the loss of continuum-like features in the ~120-400 cm^{-1} band (in the 'water'-based O atoms' spectra) vis-à-vis liquid water (cf. Fig.7), arising from immobilisation and confinement in the stable adsorption layer (cf. Fig. 4); such phenomena have also been observed at titania surfaces [16-19].

[insert Fig. 8 about here]

Focusing on the (peak-normalised) power spectra of hydrogen atoms (cf. Fig. 9), in an effort to investigate libration (rotation oscillation), H-O-H bond-bending and O-H stretch modes of the intact water molecules, it is readily evident that librational peaks of ~450-800 cm^{-1} are present, redolent of condensed phases of PBE water (also shown). It is interesting to note the much greater rôle of lower-frequency modes below ~150-200 cm^{-1} largely absent in such condensed phases (*e.g.*, the liquid); these are attributable to coupling of some water molecules' protons with the surface layer of bridging oxygen atoms, as confirmed by examination of the relevant VCCFs. There is marked suppression in bond-angle-bending motion by confinement due to adsorption, due chiefly to the relative stability of these hydrogen bonds and relative translational immobilisation of the O atoms in water due to stable electrostatic bonds with surface Fe atoms. Above ~800 cm^{-1}, however, the librational modes of the adsorbed water molecules, an integral feature of the liquid state, are essentially absent, due to confinement effects and suppression of rotation-oscillation modes naturally present in the liquid. Depending on the location, configuration and bonding arrangements of the adsorbed molecule, there is a rich tapestry of different bond-bending and bond-stretch behaviour vis-à-vis that of liquid water. For the nearest adsorbed, intact water molecule (which is involved in a hydrogen bond and an electrostatic bond to Fe), it can be

seen that the bending mode is at ~1550 cm^{-1} region, somewhat lower than PBE water, with a predicted peak at ~1690 cm^{-1} (cf. Fig. 9). However, another representative water molecule, not hydrogen-bonded directly to the surface or participating in a strong electrostatic bond, displays suppression of the bending mode, due to confinement effects. For the nearest-bound water molecule, contortions leading to qualitatively different stretch modes with respect to liquid water are intriguing. This arises from a bifurcation in behaviour, with the hydrogen-bonded proton stretch (with the surface bridging oxygen atom) shifted to the ~2000-2700 cm^{-1} region with a certain overlap or resonance between the stretch and bending mode, whilst the other proton pointing way from the hematite surface, adopts behaviour closer to that of the liquid state. Naturally, individual molecules will exhibit a 'spread of delta-spikes' about the ensemble-averaged, continuum nature of the liquid state for bond-stretch modes, so the molecule some 2 Å further away from the surface is closer to the liquid state results for O-H stretch (albeit with the already-noted marked suppression in bond-angle bending).

[insert Fig. 9 about here]

At this point, it is appropriate to remark on general mechanism for water photo-dissociation at the hematite surface, and on how the AIMD results help to inform this. Generally, with photo-excited electrons and holes produced from absorption of light in hematite's, an oxidation-reduction reaction couple takes place at the electrode's surface [53], with holes reacting with water molecules in the oxygen-evolution reaction at the anode (the hematite-water interface) [54], *i.e.*,

$$2\,h^{+} + H_2O \longrightarrow \tfrac{1}{2}\,O_2 + 2\,H^{+}$$

and electrons reducing protons at the cathode:

$2\,e^- + 2\,H^+ \longrightarrow H_2$

The AIMD simulations are most relevant to the first (oxidation) step, with an electrochemical potential of 1.23 V vis-à-vis the RHE, given that this takes place at the hematite-water interface. It would be expected that both water (O atom) and hydroxyl ions would be attracted Coulombically to Fe ions, in terms of ionic Fe-O interactions, to form the necessary close contacts (primarily by physical absorption) to allow for efficient reaction with the photo-excited holes which have diffused through the hematite to the surface. Specifically, these AIMD simulations provide insight into the dynamics of water break-up into OH^- and $H3O^+$ and also protons for hydroxylation of hematite, in addition to the necessary diffusion and rearrangement of water molecules and OH-moieties (primarily near surface Fe ions) to allow for the oxidation reaction to take place. Clearly, the intimate coupling evident in Fig. 7 of H_2O molecules (and OH^- ions in Fig. 8) with the Fe atom's translational-acoustic modes at ~90 and ~185 cm^{-1}, and some overlap of vibrational-acoustic modes at ~315 and 390 cm^{-1}, shows the value of AIMD in identifying clearly this reaction's early stages.

Conclusions

Following experimental observation of photo-driven water-splitting at hematite surfaces, the dynamical properties of (ostensibly) physically adsorbed water molecules, OH^- and H_3O^+ ions at 001-hematite surfaces have been determined from BOMD, following the establishment of partial surface-hydroxylation at room temperature. It is important to note that an alkaline electrolyte solution has been used in this study, in which OH- is present. The key link between the experimental and theoretical studies in the present work is a greater awareness of the complexities of the earlier stages of the oxygen-evolution reaction, as is evident from AIMD findings. The

rapid room-temperature surface-hydroxylation serves as evidence for the relatively low activation-energy barriers for this process, confirming previous experimental and simulation findings [31, 32, 35, 36]. A relatively stable configuration emerges (vis-à-vis the ~10 ps time-scale of the simulations), albeit one featuring proton transfer in the adsorption layer amongst some of the water molecules and OH^- and H_3O^+ ions. It has been found that there is substantial coupling of O atoms in intact water molecules or hydroxyl ions with Fe atoms, due to electrostatic bonding, from examination of respective VACF- and VCCF-spectra. Hydrogen-bonding of aqueous protons to bridging oxygen atoms at the surface are also important, which can lead to perturbations in O-H stretch and H-O-H bending modes. It has been seen that there is a rich physico-chemical diversity of behaviour at water-hematite interfaces. It is to be hoped that non-adiabatic MD may, in the future, offer the potential to model the dynamics of photo-excited electron injection directly, where the already-evident subtleties of phonon-coupling (from the present study) will no doubt affect the ballet of photo-excited electron-phonon coupling into the conduction-band manifold of the hematite.

Acknowledgments

This work was supported by the Science Foundation Ireland (SFI) Research Frontiers Programme (reference No. 10/RFP/MTR2868) and Strategic Research Cluster on Advanced Biomimetic Materials for Solar Energy Transformation (reference No. 07/SRC/B1160). The authors thank SFI and the Irish Centre for High End Computing for the provision of computational resources, and also the PRACE DECI 7 programme for generous access to the Bull Nehalem cluster at HLRS in Stuttgart, and staff at ICHEC and HLRS.

References

(1) Fujishima, A.; Honda, K. *Nature***1972**, *238*, 37.

(2) Haller, G.L.; Resasco, D.E., *Adv. Catalysis***1989**, *36*, 173.

(3) K. M. Rosso, D. M. A. Smith, and M. Dupuis, J. Chem. Phys. **118**, 6455 (2003).

(4) J. A. Glasscock, P. R. F. Barnes, I. C. Plumb, and N. Savvides, J. Phys.Chem. C **111**, 16477 (2007).

(5) Y. S. Hu, A. Kleiman-Shwarsctein, G. D. Stucky, and E. W. McFarland, Chem. Commun. (Cambridge) 2009, 2652.

(6) Y. S. Hu, A. Kleiman-Shwarsctein, A. J. Forman, D. Hazen, J. N. Park, and E. McFarland, Chem. Mater. **20**, 3803 (2008).

(7) A. Kleiman-Shwarsctein, Y.-S. Hu, A. J. Forman, G. D. Stucky, and E. W. McFarland, J. Phys. Chem. C **112**, 15900 (2008).

(8) A. Kleiman-Shwarsctein, Y.-S. Hu, G. D. Stucky, and E. W. McFarland, Electrochem. Commun. **11**, 1150 (2009).

(9) W. B. Ingler, J. P. Baltrus, and S. U. M. Khan, J. Am. Chem. Soc. **126**, 10238 (2004).

(10) S. Kumari, C. Tripathi, A. P. Singh, D. Chauhan, R. Shrivastav, S. Dass, and V. R. Satsangi, Curr. Sci. **91**, 1062 (2006).

(11) Diebold, U. *Surf. Science Reports* **2003**, *48*, 53.

(12) Henderson, M.A., *Surf. Science Reports* **2002**, *46*, 1.

(13) Sun, C., et al., *J. Mater. Chem.* **2010**, *20*, 10319, and references therein.

(14) Mattioli, G.; Filippone, F.; Caminiti, R.; Bonapasta, A. A. *J. Phys. Chem. C***2008**, *112*, 13579.

(15) Kavathekar, R.; Dev, P.; English, N.J.; MacElroy, J.M.D. *Molec. Phys.* **2011**, *109*, 1649.

(16) Kavathekar, R.; English, N.J.; MacElroy, J.M.D., *Molec Phys.* **2011**, *109*, 2645.

(17) English, N.J.; Kavathekar, R.; MacElroy, J.M.D., *Molec Phys.*,**2012**, *110*, 2919-2925.

(18) Zhang, Z.; P. Fenter; L. Cheng; N. C. Sturchio; M. J. Bedzyk; M. Předota; A. Bandura; J. D. Kubicki; S. N. Lvov; P. T. Cummings; A. A. Chialvo; M. K. Ridley; P. Bénézeth; L. Anovitz; D. A. Palmer; M. L. Machesky; D. J. Wesolowski, *Langmuir***2004**, *20*, 4954.

(19) Predota, M; Bandura, AV; Cummings, PT; Kubicki, JD; Wesolowski, DJ; Chialvo, AA; Machesky, ML, *J. Phys. Chem. B*, **2004**, *108*, 12049.

(20) Predota, M.; P. T. Cummings; Z. Zhang; P. Fenter; D. J. Wesolowski, *J. Phys. Chem. B*, **2004**, *108*, 12061.

(21) Predota, M.; P. T. Cummings; D. J. Wesolowski, *J. Phys. Chem. C*, **2007**, *111*, 3071.

(22) Machesky ML; Predota M; Wesolowski DJ; Vlcek L; Cummings PT; Rosenqvist J; Ridley MK; Kubicki JD; Bandura AV; Kumar N; Sofo JO, *Langmuir*, **2008**, *24*, 12331.

(23) Kavathekar, R.; English, N.J.; MacElroy, J.M.D., *Chem. Phys. Lett.* **2012**, *554*, 102-106

(24) Cheng, J.; Sprik, M. *J. Chem. Theory Comput.* **2010**, 6, 880-889.

(25) Aschauer, U.; He, Y.; Cheng, H.; Li, S.-C.; Diebold, U.; Selloni, A., *J. Phys. Chem. C*, **2010**, *114*, 1278–1284

(26) Cheng, H.; Selloni, A., *Langmuir*, **2010**, *26(13)*, 11518–11525

(27) Tilocca, A.; Selloni, A.,*J. Phys. Chem. C*, **2012**, *116*, 9114−9121

(28) Aschauer, U.; Selloni, A., Phys. Rev. Lett. **2011**, *106*, 166102.

(29) Kumar, N.; Neogi, S.; Kent, P. R. C.; Bandura, A. V.; Kubicki, J. D.; Wesolowski, D. J.; Cole, D.; Sofo, J. O. *J. Phys. Chem. C* **2009**, *113*, 13732.

(30) English, N.J., *Chem. Phys. Lett.* **2013**, *583*, 125-130

(31) Rohrbach, A.; Hafner, J.; Kresse, G.,*Phys. Rev. B* **2004**, *70*, 125426.

(32) Bergermayer, W.; Schweiger, H.; Wimmer, E.,*Phys. Rev. B* **2004**,*69*, 195409.

(33) Yin, S.; Ma, X.; Ellis, D.E.,*Surf. Sci.* **2007**, *601*, 2426.

(34) Trainor, T.P.; Chaka, A.M.; Eng, P.J.; Newville, M.; Waychunas, G.A.; Catalano, J.G.; Brown, G.E., Jr., *Surf. Sci.* **2004**,*573*, 204.

(35) Kubicki, J.D.; Paul, K.W.; Sparks, D.L., Geochem. Trans. **2008**, *9*, 4.

(36) Nguyen,M.-T.; Seriani, N.; Gebauer, R., *J. Chem. Phys.* **2013**, 138, 194709

(37) Liu, C.Z.; Thornton, G.; Michaelides, A., *Phys. Rev. B* **2010**, *82*, 161415.

(38) Wesolowski, D.J., Sofo, J.O., Bandura, A.V., Zhang, Z., Mamontov, E., Předota, M., Kumar, N., Kubicki, J.D., Kent, P.R.C., Vlcek, L., Machesky, M.L., Fenter, P.A., Cummings, P.T., Anovitz, L.M., Skelton, A.A., and J. Rosenqvist, *Phys. Rev. B* **2012**, *85*, 167401.

(39) Li, M.L., C. Zhang, G. Thornton and A. Michaelides, *Phys. Rev. B* **2012**, *85*, 167402.

(40) Rahman, M.; Wadnerkar, N.; English, N.J.; MacElroy, J.M.D. 'The influence of Ti and Si doping on the structure, morphology and photo-response properties of α-Fe_2O_3 for efficient water splitting: experiment and first-principle calculations', *Chem. Phys. Lett.* (in press); DOI: http://dx.doi.org/10.1016/j.cplett.2013.12.021

(41) A. Kay, I. Cesar and M. Gratzel, J. Am. Chem. Soc., 2006, 128, 15714-15721

(42) Rahman,M.; MacElroy, J.M.D.;Dowling, D.P.,*J. Nanosci. Nanotechnol.***2011**, 8642-8651.

(43) Rahman, M.; Dang, B.H.Q.; McDonnell, K.; MacElroy, J.M.D.; Dowling, D.P.,*J. Nanosci. Nanotechnol.*, **2012**, 12, 4729-4735.

(44) H. J. C. Berendsen, J. R. Grigera, and T. P. Straatsma. *J. Phys. Chem.* **1987**, *91*, 6269.

(45) Blöchl, P. E. *Phys. Rev. B* **1994**, *50*, 17953.

(46) Kresse, G.; Furthmuller, J. *Phys. Rev. B* **1996**, *54*, 11169.

(47) J. P. Perdew, K. Burke, M. Ernzerhof, *Phys. Rev. Lett.* **1996**, *77*, 3865.

(48) Allen, M. P.; Tildesley, D. J. *Computer Simulation of Liquids*; Oxford, 1987.

(49) Reece, S.Y.; Hamel, J.A.; Sung, K.; Jarvi, T.D.; Esswein, A.J.; Pijpers, J.J.H.; Nocera, D.G., Science **2011**, *334*, 6056.

(50) Liu, Z.; Pesic, B.; Raja, K.S.; Rangaraju, R. R.; Misra, M., Internat. J. Hydrogen Energy**2009**, 34, 3250-3257

(51) Brillet,J.; Yum, J.; Cornuz, M.; Hisatomi, T.; Solarska, R.; Augustynski, J.; Grätzel, M.; Sivula, K., Nature Photonics 2012,*6*, 824–828.

(52) Pascal, T.A.; Schärf, D.; Jung, Y.L Kühne, T., *J. Chem. Phys.* **2012**, *137*, 244507.

(53) Harrison, K.W.; Remick, R.; Martin, G.D.; Hoskin, A. 'Hydrogen Production: Fundamentals and Case-Study Summaries', in 'Hydrogen and Fuel Cells', Stolten, D., (Ed.); Wiley: Weinheim, 2010.

(54) Kudo, A.; Kato, H.; Tsuji, I., Chem. Lett. **2004**, *33*, 1534.

Figure Captions

Fig 1: X-Ray diffraction spectrum of FTO substrate and hematite thin film on FTO substrate. Shown also are standard hematite (JCPDS 00-001-1053) peak positions. Note: For Hematite, electron conduction is strongly favoured along the (001) basal plane with hole conduction taking place within the (110) plane.

Fig 2: Current-voltage curve of the hematite photoanode under darkness and simulated sunlight measured in three electrodes photoelectrochemical cell using 1M NaOH as a electrolyte.

Fig 3: Experimental evidence of solar driven water splitting process on hematite surface (a) before and (b) after turning on light.

Fig 4:Snapshots of the interfaces at various times from MD. The larger red spheres denote Fe atoms, whilst the small red ones represent oxygen atoms (in either the hematite or water). The (blue) hydrogen atoms have not been 'imaged' periodically to place them near the corresponding oxygen atoms in intact water molecules. (1) Shows the system just after DFT-level geometry optimisation, with strong electrostatic contacts shown explicitly between three surface Fe atoms and oxygen atoms in three water molecules. (2) After ~0.5ps, the 'shaded' water molecule has become more H_3O^+ in character, with the nearby 'electrostatically bound' water molecule (on the right) having transferred its proton thereto (and thus become more negatively charged, *i.e.*, more OH^- in character). (3) After ~0.6ps, the shaded, transient H_3O^+ species is attracted (electrostatically) to a hematite surface oxygen atom, whereupon it 'gives up' one of its protons thereto to form a chemical bond (achieving initial, partial hydroxylation of the hematite surface). (4) After ~1 ps, the former shaded H_3O^+ species has 'reverted' to a water molecule (albeit with a different pair of protons than at the outset), with its two protons oriented away from the surface-bound proton. Snapshots (5) to (9) are after ~3, 5, 7, 9 and 11 ps, respectively, which show that this structure remains stable, with 'formal' hydroxylation with the shaded proton, but also *de facto* modification of the surface by physico-chemical electrostatic, or ionic, bonds with either water molecules or OH^- species (for stronger Fe-O ionic bonds in the latter case),

which are, on occasion, wont to swop protons with surrounding water molecules (rendering them transient $H3O^+$ moieties in their midst). Note also that after ~2-3ps (*i.e.*, between snapshots (4) and (5)), that there is greater dipolar alignment of the water molecules at the 'top' of the simulation box, which are forming transient hydrogen bonds with the oxygen atoms at the 'bottom' of the hematite surface (shown in snapshot (1)); the required reorientation of the water molecules from the initial bulk-like water configuration in (1), albeit relaxed, takes ~3 ps. As an example, in snapshot (6), the dipole vectors of the water molecules at the 'top' of the box are shown in green, with four of the five aligned approximately towards the bottom of the hematite surface.

Fig 5: Water-oxygen density profile with respect to *z*-axis position in the simulation box, with 0 Å denoting the 'bottom' surface of the hematite, 13 Å the approximate position of the studied interface, and ~25-26 Å the 'top' of the box; cf. Fig. 1(1). The 'slices' are of 0.5 Å in width. The grey lines denote the initial configuration (before any geometry-optimisation), whilst the dotted black line is derived from the trajectory after the first picosecond (*i.e.*, in the relatively stable post-hydroxylation structure). In this latter case, the closer contact of 'water' molecules (or OH^- moieties) with Fe due to electrostatic interactions is clear, with greater evidence of more pronounced hematite-induced 'layering' in the water structure relative to the bulk liquid; this is also the case with a distinct layer at~24-26 Å at the second interface with the 'bottom' hematite surface in Fig. 1(1).

Fig 6: Vibrational density of states (from peak-normalised VACF power spectra) of the Fe and O atoms in hematite in the 'top' layer in contact with the physically- and chemically-adsorbed water molecules, after 1 ps; cf. Fig. 1(1).

Fig 7: Vibrational density of states (from peak-normalised VACF power spectra) of O atoms in physically-adsorbed water molecules at the hematite surface. That of bulk water is also shown. The dotted line is the closest water molecule (for which there is stable hydrogen-bonding with the bridging oxygen, and electrostatic interaction with nearby Fe atoms), while dotted grey is around 2 Å 'further out', where these more explicit interactions with the hematite are much weaker. A molecule near the 'middle' of the liquid layer in between the two interfaces is also shown. These are depicted in the inset snapshot.

Fig 8: Vibrational density of states (from peak-normalised VACF power spectra) of O atoms in OH^- (dotted) and $H3O^+$ moieties (dashed-grey and continuous). The OH^- is physically adsorbed, with interactions with Fe, whilst the dashed-grey $H3O^+$ is hydrogen-bonded to a bridging oxygen atom. The continuous-black $H3O^+$ is around 1.5 Å further from the surface with less explicit physical interaction.

Fig 9: Vibrational density of states (from peak-normalised VACF power spectra) of H atoms in physically-adsorbed water molecules at the hematite surface. That of bulk water is also shown. The dotted line is the closest water molecule (for which there is stable hydrogen-bonding with the bridging oxygen, and electrostatic interaction with nearby Fe atoms), while dotted grey is around 2 Å more distant from the surface, where these more explicit interactions with the hematite are substantially weaker. Both of these are depicted in the inset snapshot in Fig. 7.

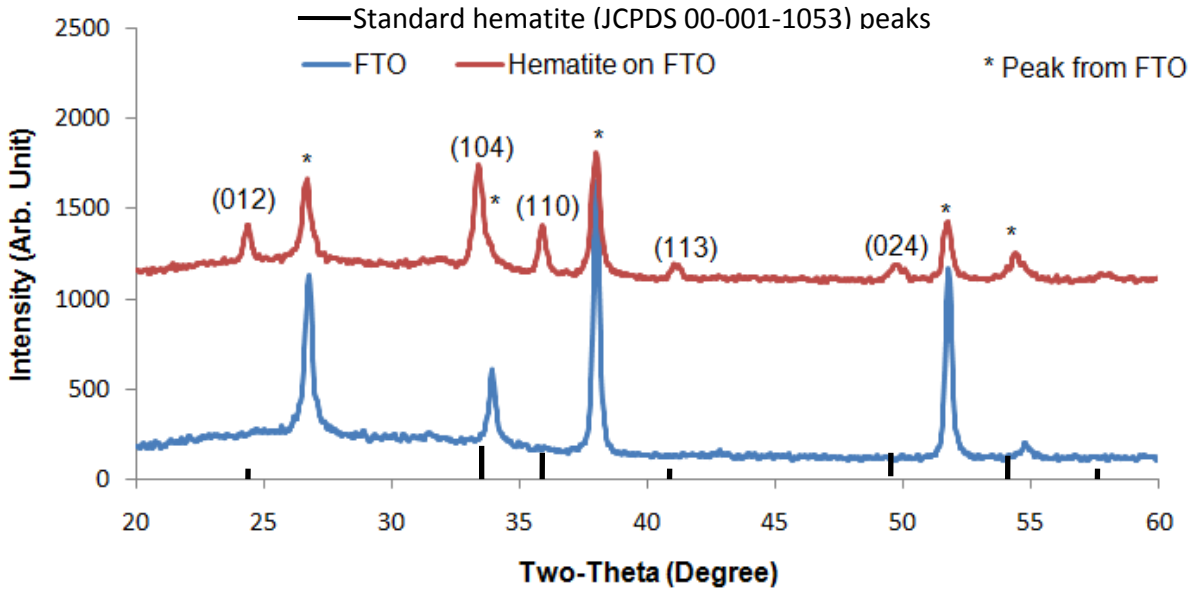
Standard hematite (JCPDS 00-001-1053) peaks
FTO
Hematite on FTO
* Peak from FTO
Intensity (Arb. Unit)
Two-Theta (Degree)
(012)
(104)
(110)
(113)
(024)
2500
2000
1500
1000
500
0
20
25
30
35
40
45
50
55
60

Fig. 1

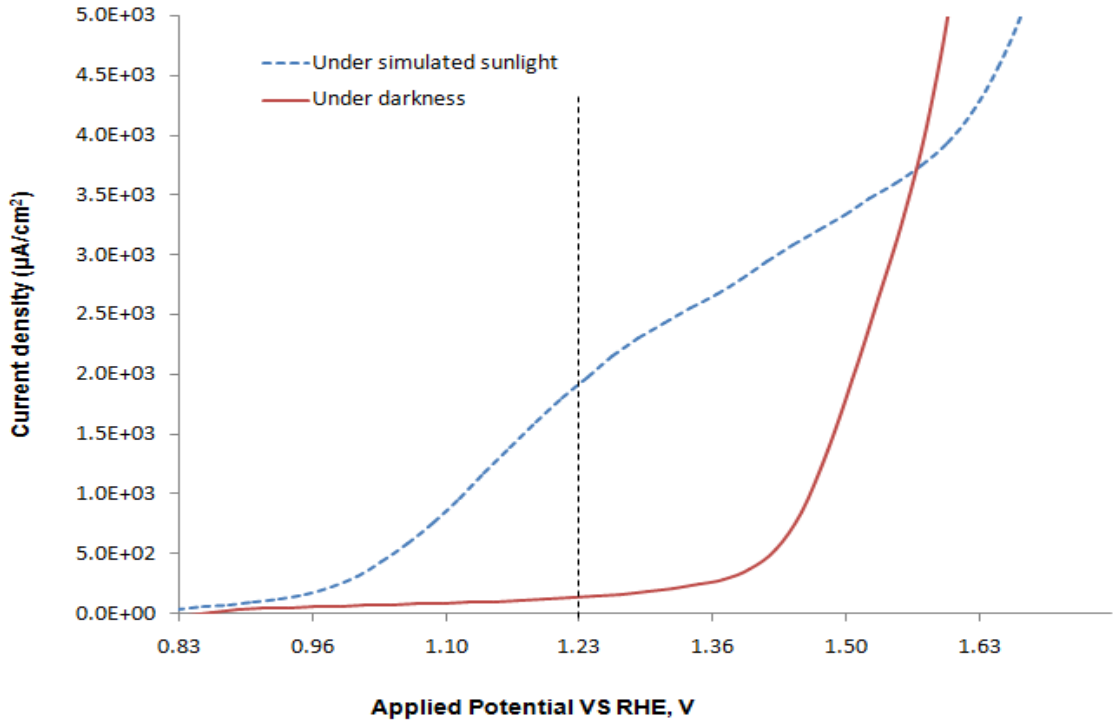
5.0E+03
4.5E+03
4.0E+03
3.5E+03
3.0E+03
2.5E+03
2.0E+03
1.5E+03
1.0E+03
5.0E+02
0.0E+00
Current density (μA/cm²)
Under simulated sunlight
Under darkness
0.83
0.96
1.10
1.23
1.36
1.50
1.63
Applied Potential VS RHE, V

Fig. 2

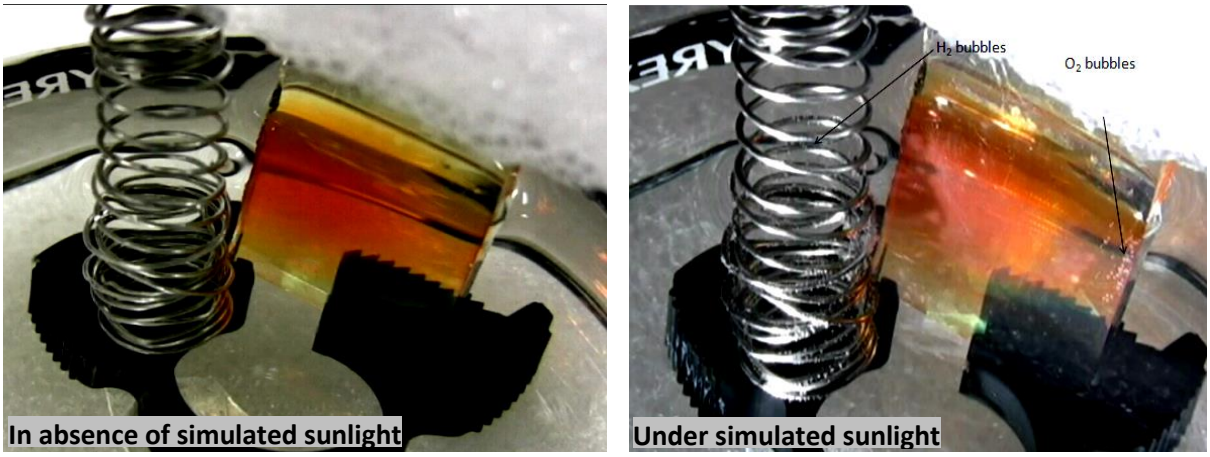
In absence of simulated sunlight
H_2 bubbles
O_2 bubbles
Under simulated sunlight

(a) (b)

Fig. 3

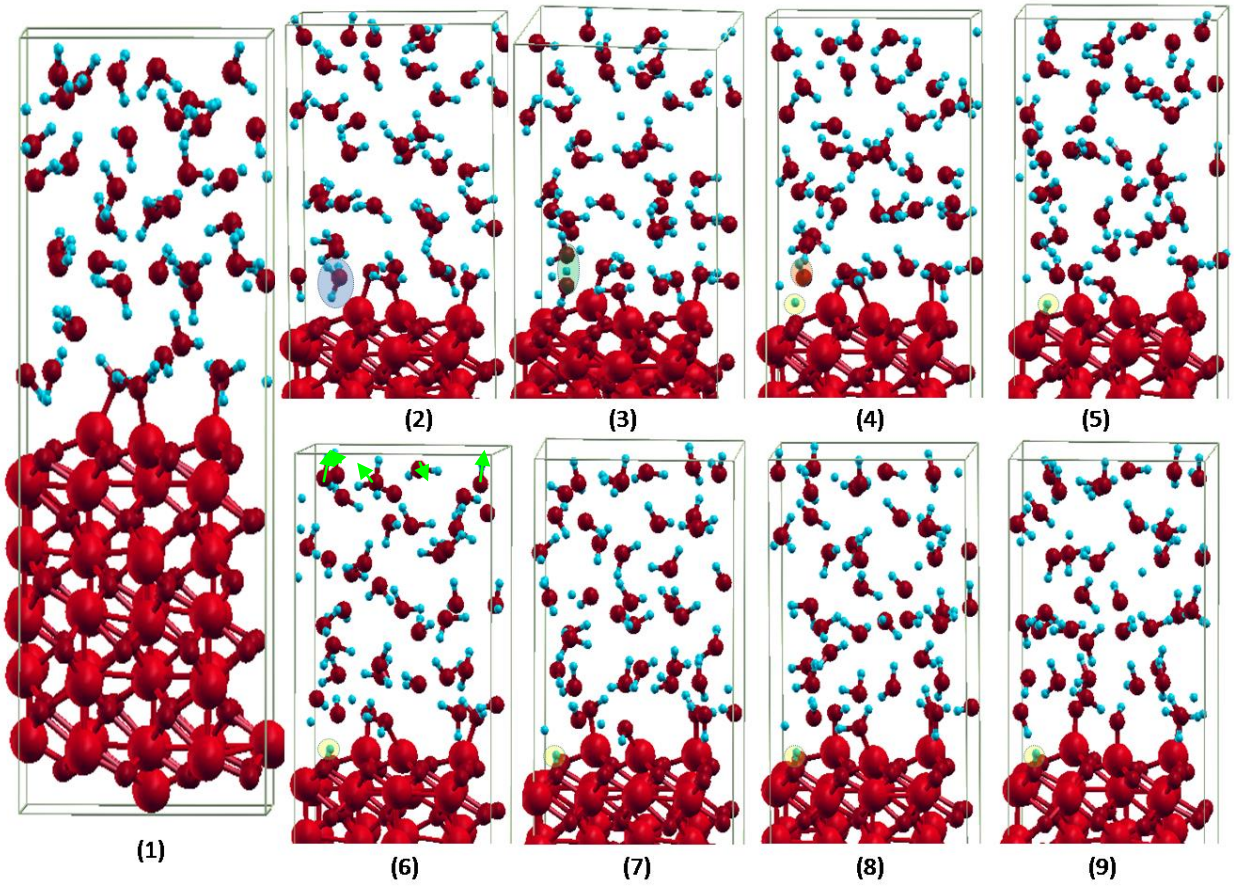

Fig. 4

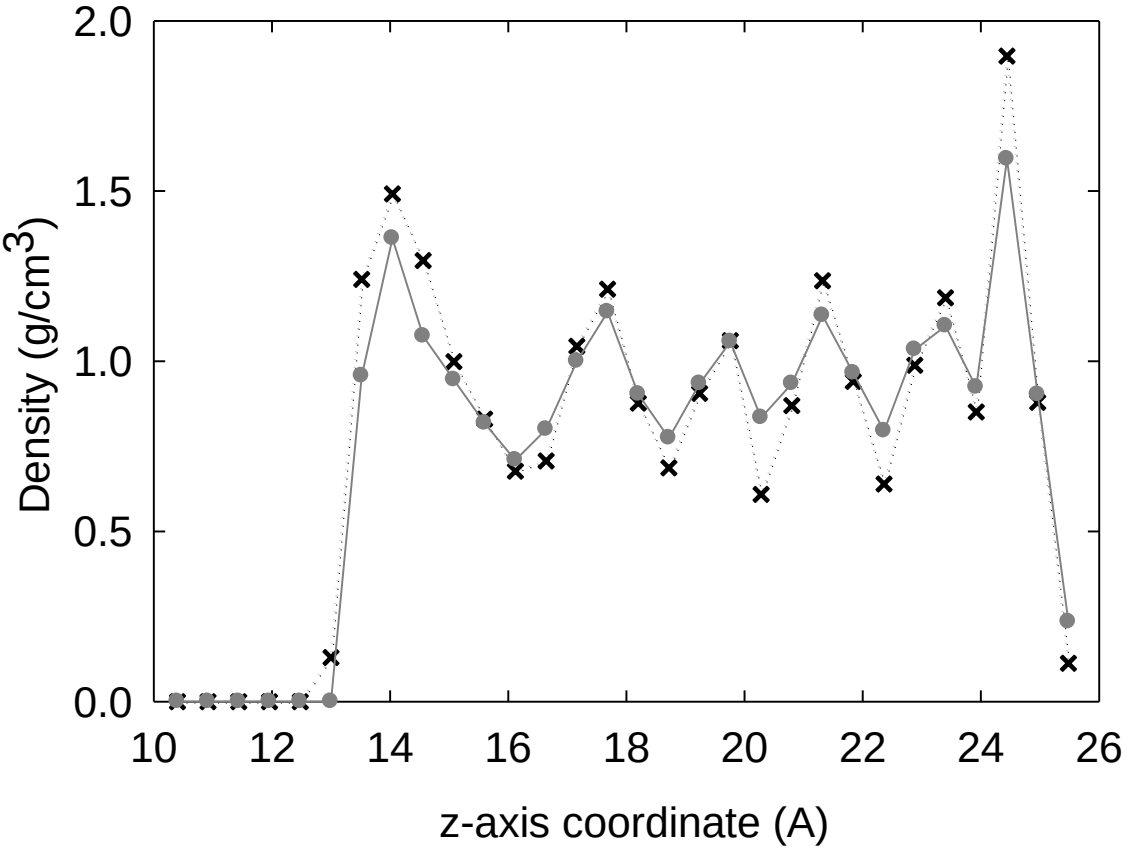
2.0
1.5
1.0
0.5
0.0
Density (g/cm3)
10
12
14
16
18
20
22
24
26
z-axis coordinate (A)

Fig. 5

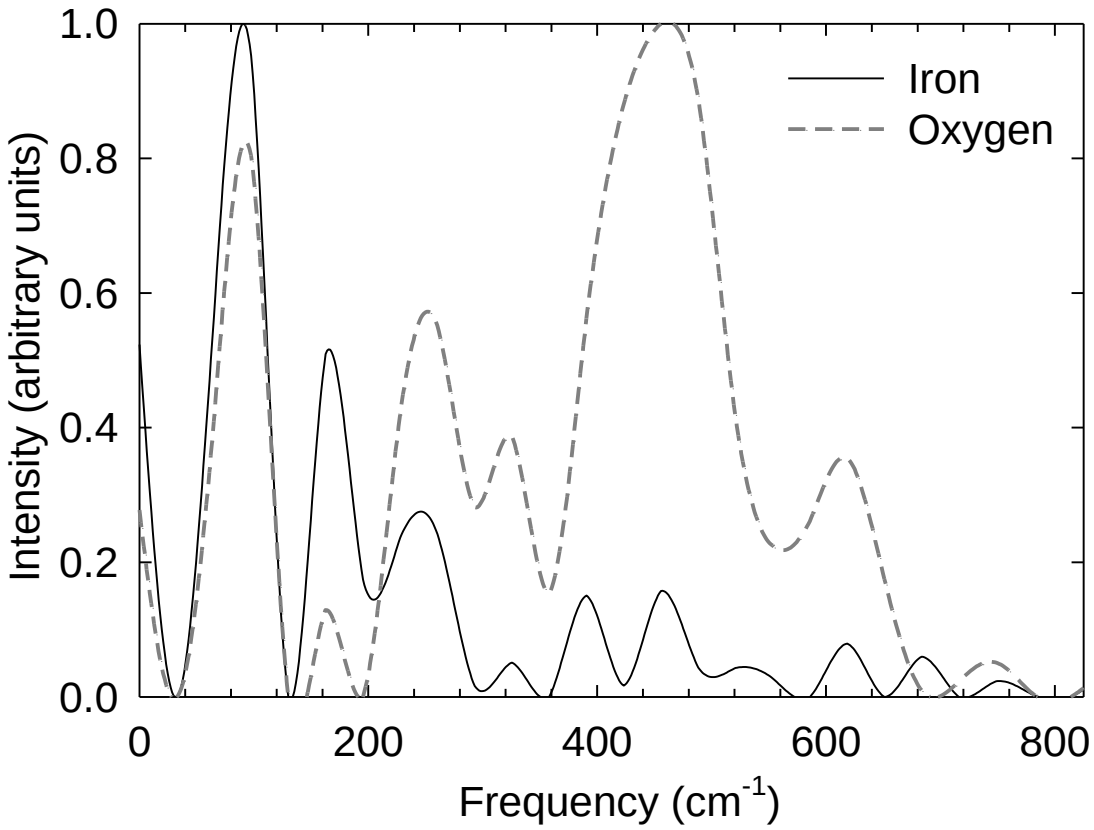
1.0
0.8
0.6
0.4
0.2
0.0
Intensity (arbitrary units)
0
200
400
600
800
Frequency (cm-1)
Iron
Oxygen

Fig. 6

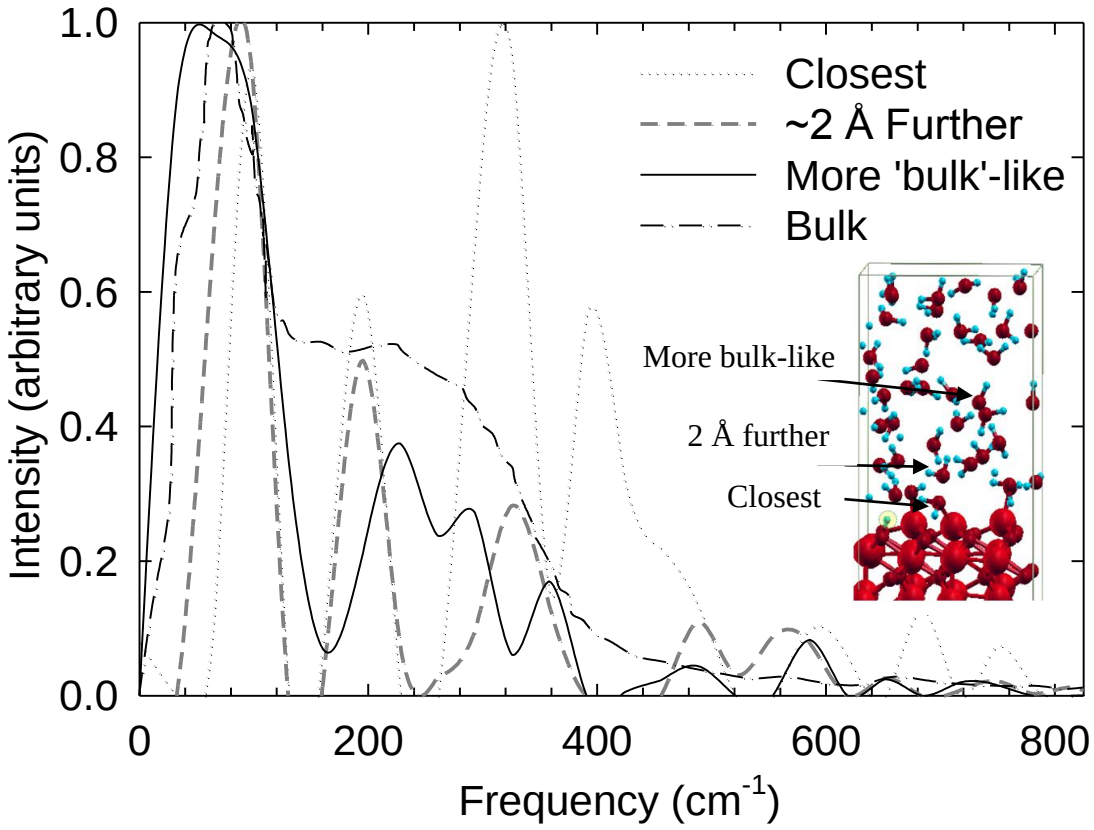
1.0
0.8
0.6
0.4
0.2
0.0
Intensity (arbitrary units)
0
200
400
600
800
Frequency (cm-1)
Closest
~2 Å Further
More 'bulk'-like
Bulk
More bulk-like
2 Å further
Closest

Fig. 7

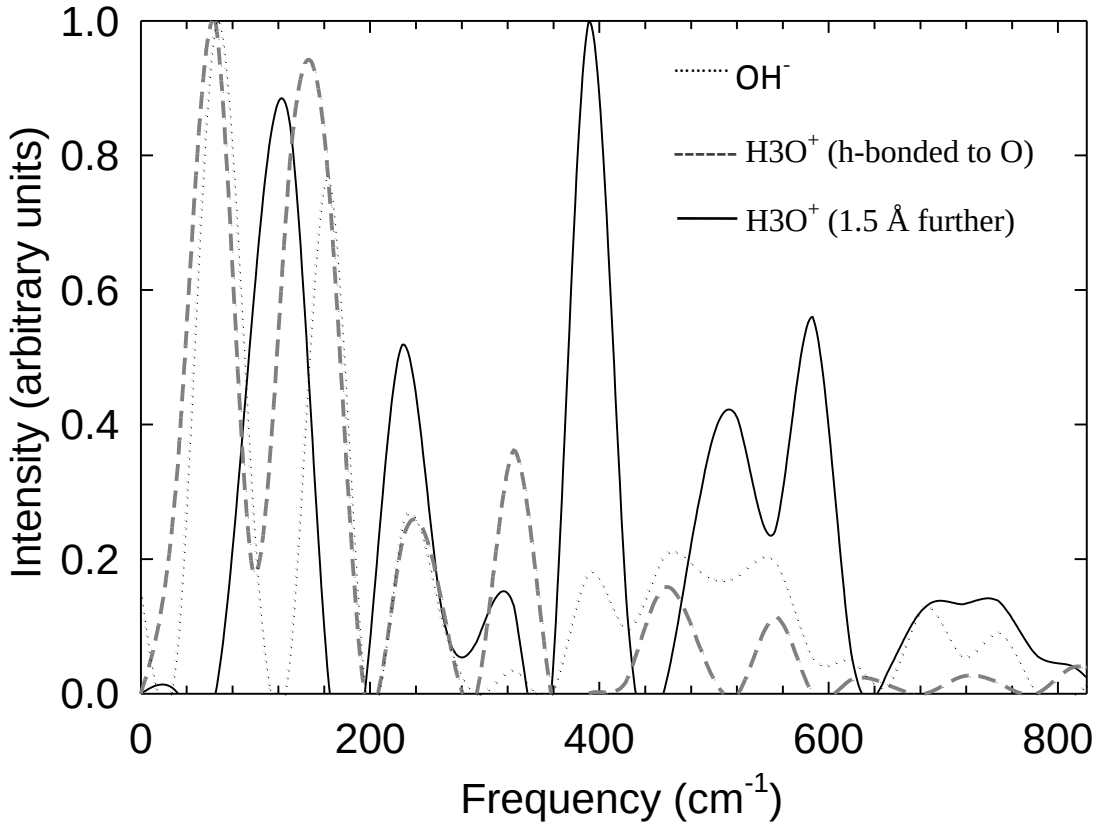
1.0
0.8
0.6
0.4
0.2
0.0
Intensity (arbitrary units)
0
200
400
600
800
Frequency (cm-1)
OH-
H3O+ (h-bonded to O)
H3O+ (1.5 Å further)

Fig. 8

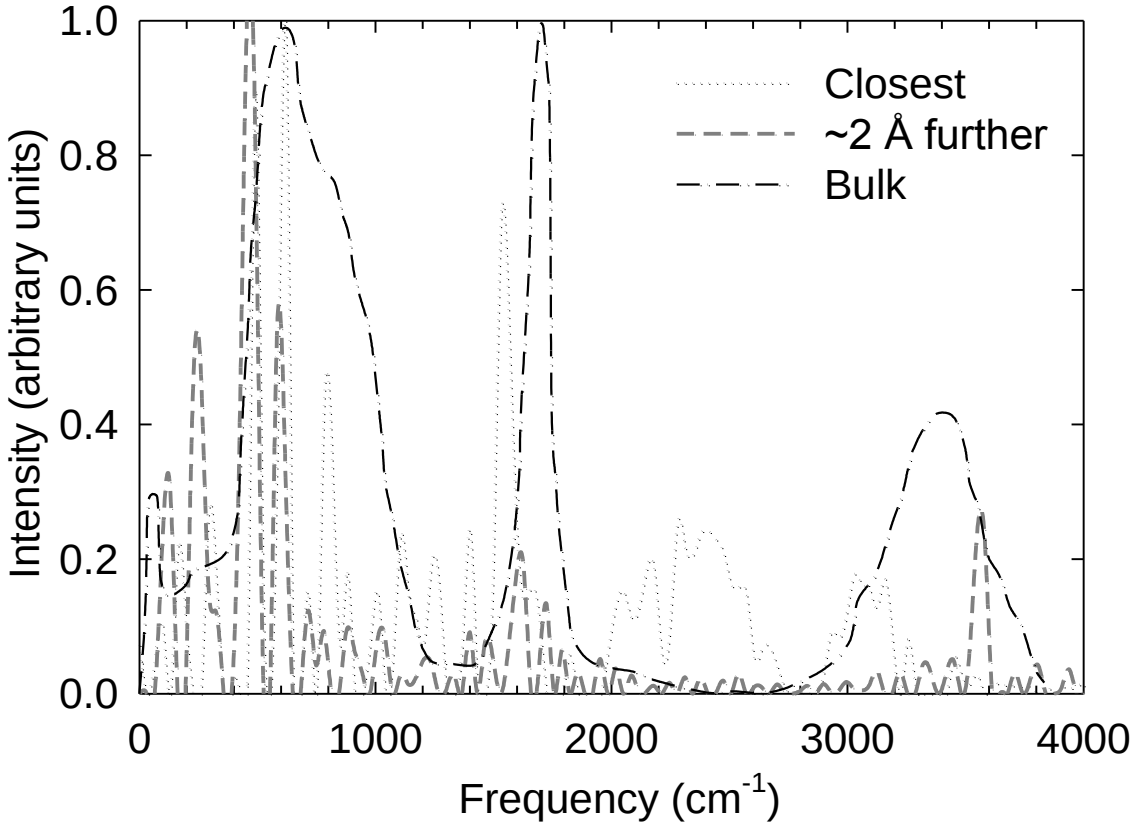
1.0
0.8
0.6
0.4
0.2
0.0
Intensity (arbitrary units)
0
1000
2000
3000
4000
Frequency (cm-1)
Closest
~2 Å further
Bulk

Fig. 9